Journal of Magnetism and Magnetic Materials 614 (2025) 172766

Contents lists available at ScienceDirect

Journal of Magnetism and Magnetic Materials

journal homepage: www.elsevier.com/locate/jmmm

# Giant magnetocaloric properties of Gd-based double perovskite compounds in cryogenic temperature range

Meenakshi [a], Sanjay Saini [b], Neeraj Panwar [c], Ramovatar [a,*], Surendra Kumar [d,*]

[a] Department of Physics and Astrophysics, Central University of Haryana, Mahendergarh, Haryana, 123031, India
[b] Materials Science Division, Bhabha Atomic Research Centre, Trombay, Mumbai, 400085, India
[c] Department of Physics, Chaudhary Charan Singh University, Meerut, Uttar Pradesh, 250004, India
[d] Department of Physics, Shivaji College, University of Delhi, New Delhi, 110027, India

ARTICLE INFO

*Keywords:*
Double Perovskite
Magnetic Refrigeration
Magnetocaloric Effect
Transition Temperature

ABSTRACT

Magnetic refrigeration technology (MRT) leverages the magnetocaloric effect (MCE) to deliver an innovative, energy-efficient, and eco-friendly cooling solution. The primary challenge in advancing MRT lies in optimizing materials with a robust MCE and developing practical systems for widespread refrigeration and cooling applications. In this study, a double perovskite-structured $Gd_2FeCrO_6$ (GDFCO) compound is synthesized following the conventional sol–gel technique and its structural, microstructural, and magnetocaloric properties are examined. The X-ray diffraction (XRD) analysis along with Rietveld refinement, confirms the presence of two coexisting phases, monoclinic structure with $P2_1/n$ space group (90.94 %) and minimal amount of trigonal structure with $R\bar{3}\,c$ space group (9.06 %). The average crystallite size, determined from the Williamson-Hall plot, is ~ 120 nm. Field Emission Scanning Electron Microscopy (FESEM) image reveals a homogeneous microstructure with nearly spherical shapes, while Energy Dispersive X-ray Spectroscopy (EDS) verifies the presence and correct proportion of required elements. The compound exhibits two magnetic transition temperatures, with $T_{N1}$ occurring at ~ 220 K and $T_{N2}$ at ~ 6 K. Arrott's plot conforms to the second-order phase transitions (SOPT). A remarkable magnetocaloric effect (MCE) was observed, with a maximum entropy change ($-\Delta S_M$) ~ 38.6 J/kg K and relative cooling power (RCP) ~ 418 J/kg at 4 K with applied magnetic fields of 0–70 kOe. These findings indicate that GDFCO can be a better material for cryogenic magnetic refrigeration, with the potential to advance the field of magnetic cooling technology.

## 1. Introduction

The rapid industrial growth and the rise in global population have led to growing demand for efficient and sustainable cooling technologies [1,2]. Magnetic refrigeration, an emerging technology in the field of cooling systems, offers a promising alternative to traditional gas-compression based refrigeration that relies on volatile refrigerants, which contribute to global warming and ozone depletion. Magnetic refrigeration utilizes solid-state materials, eliminating the need for harmful gases and potentially improving energy efficiency [3,4]. The solid-state approach not only reduces environmental impact but also offers the possibility of quieter, more reliable, and compact cooling systems. Magnetic refrigeration exploits the magnetocaloric effect (MCE), a phenomenon where certain materials experience, entropy or temperature change when exposed to varying magnetic fields [5]. However, a considerable gap persists between the laboratory development of these materials and their practical applications. As a result, the search and design of suitable magnetocaloric materials continue to be the primary objectives in this field. Among the various classes of magnetocaloric materials, rare-earth based double perovskite oxides have garnered considerable attention owing to their diverse physical and chemical properties [1,6–9]. These materials exhibit unique characteristics such as magnetic field-induced metamagnetic transitions, multiferroic behaviour, temperature-induced magnetization reversal, and significant magnetocaloric effects (MCE), making them highly promising for advanced technological applications, particularly in magnetic refrigeration [7,10–19]. The chemical formula of the double perovskites is denoted by the $RE_2BB'O_6$, where *RE* represents a rare-earth element, *B* and *B'* are two distinct transition metal cations [20,21]. Due to the broad selection of *B* and *B'* cations available across the periodic table, the

* Corresponding authors.
*E-mail addresses:* ramovatar@cuh.ac.in (Ramovatar), surendrakumar@shivaji.du.ac.in (S. Kumar).

https://doi.org/10.1016/j.jmmm.2024.172766
Received 18 October 2024; Received in revised form 13 December 2024; Accepted 29 December 2024
Available online 30 December 2024

electronic structure, and magnetic properties of these materials can be precisely tuned [12,20–24].

Recently, rare-earth based single and double perovskites have attracted much attention for their better magnetocaloric properties, offering great potential for advancing magnetic refrigeration technology. Wang *et al.* reported excellent magnetocaloric effects (MCE) in $GdCrO_3$ and $DyCrO_3$ compounds with maximum entropy change ($\Delta S_M$) ~ 39.9 J/kg K and 15.9 J/kg K, and maximum adiabatic temperature change ($\Delta T_{ad}$) ~ 18.18 K and 10.58 K, respectively, under a 50 kOe applied magnetic field. They also achieved the corresponding refrigerant capacity (RCP) values ~ 373.4 J/kg and ~ 276 J/kg, respectively for $GdCrO_3$ and $DyCrO_3$ compounds [25]. In another study on $Ho_2CrMnO_6$ and $Er_2CrMnO_6$ compounds, $\Delta S_M$ ~ 11.03 J/kg K and 12.94 J/kg K were achieved with RCP values of 322.7 J/kg and 277.5 J/kg, respectively across a magnetic field range of 0–7 T [26]. Prusty *et al.* synthesized the $Dy_{1-x}Gd_xMnO_3$ ($0 \leq x \leq 1$) compositions and examined their structural, electronic, and magnetocaloric properties. Their study revealed that increasing the Gd concentration led to a significant enhancement in the magnetocaloric properties of these compounds. They reported that the maximum entropy change was almost two times ~ 15.35 J/kg K in $Dy_{0.5}Gd_{0.5}MnO_3$ composition as compared to that of the pristine compound, where $\Delta S_M$ ~ 7.48 J/kg K was achieved. The RCP value for $Dy_{0.5}Gd_{0.5}MnO_3$ compound was ~ 307 J/kg, whereas it was ~ 174 J/kg for the $DyMnO_3$ sample at 9 T magnetic field [27]. Shi *et al.* also highlighted the enhancement of magnetocaloric properties in $ErCrO_3$ composition through Gd substitution at the *A*-site. They observed that $\Delta S_M$ increased from 10.7 J/kg K in $ErCrO_3$ to 27.6 J/kg K in $Er_{0.33}Gd_{0.67}CrO_3$, while RCP values increased from 416.4 J/kg to 531.1 J/kg, respectively under 7 T applied magnetic field [28]. Murthy *et al.* conducted a comparative study of the magnetocaloric effect in $Gd_2BMnO_6$ ($B$ = Ni and Co) compounds, observing ferromagnetic ordering at 130 K and 112 K, with the maximum entropy changes $\Delta S_M$ ~ 35.5 J/ kg K and ~ 24 J/kg K in $Gd_2NiMnO_6$ and $Gd_2CoMnO_6$, respectively [29]. These findings demonstrate that Gd substituted or Gd-based compounds exhibit significant magnetocaloric effect due to the large magnetic moment associated with $Gd^{3+}$ (7 $\mu_B$) and quenched orbital momentum. Thus Gd-based perovskites are promising candidates for next-generation magnetic refrigeration technologies.

In particular, $R_2FeCrO_6$ compounds exhibit captivating magnetic properties due to the coexistence of two transition metal ions, $Fe^{3+}$ and $Cr^{3+}$ [30,31]. Based on the Goodenough-Kanamori rules, these compounds are anticipated to exhibit ferromagnetic order due to the 180° superexchange interaction between $Fe^{3+}$ and $Cr^{3+}$ ions connected by oxygen [32,33]. This theoretical prediction is supported by numerous studies, including the exploration of multiferroic properties in compounds like $Bi_2FeCrO_6$ and $Pr_2FeCrO_6$ [34,35]. Notably, $R_2FeCrO_6$ compounds ($R$ = La, Nd) have demonstrated temperature-induced magnetization reversal and magnetic switching effects, while $Y_2FeCrO_6$ nanocrystals have shown a significant magnetodielectric effect [36,37]. A remarkable magnetization reversal of –12 emu/mol, accompanied by a high compensation temperature ($T_{COMP}$) of ~ 192 K, along with sign reversal in both conventional and spontaneous exchange bias fields was obtained by Patra *et al.* [38]. Further investigations on $Dy_2FeCrO_6$ revealed a magnetic transition from paramagnetic to antiferromagnetic state, with Néel temperature ($T_N$) of 15.5 K, and the corresponding magnetocaloric properties characterized by a change in $\Delta S_M$ of ~ 12.64 J/kg K and RCP value of ~ 241.4 J/kg under a 5 T magnetic field [11]. Huang *et al.* studied the $Tb_2FeCrO_6$ oxide and observed the magnetocaloric effects with $\Delta S_M$ and *RCP* values of ~ 12.9 J/kg K and ~ 341.4 J/kg, respectively under 7 T magnetic field [39]. Bhuyan *et al.* developed $Gd_2FeCrO_6$ nanomaterial and obtained the absence of a sharp magnetic transition, indicating a lack of long-range magnetic ordering between $Fe^{3+}$ and $Cr^{3+}$ ions. They also carried out the first principles calculations on $Nd_2CrFeO_6$ and $Gd_2FeCrO_6$ compounds and predicted the ferrimagnetic nature of these materials [40–42]. These studies highlight the diverse and complex magnetic behaviour in the $R_2FeCrO_6$ double-perovskites family, sparking significant interest in their potential applications in magnetocaloric, spintronics, and other advanced magnetic technologies. Despite the promising attributes of $R_2FeCrO_6$ double-perovskites, the magnetocaloric effect (MCE) of these materials remains largely unexplored which offers an exciting opportunity for future research.

The intriguing magnetic properties of Gd-based double perovskites motivated us to study these materials. Therefore, in this study, the $Gd_2FeCrO_6$ compound was synthesized using the conventional sol–gel method, and its structural and magnetic properties were investigated, with a particular focus on the magnetocaloric effect, in an effort to further advance the development of materials for cryogenic magnetic refrigeration application.

## 2. Experimental procedures

### 2.1. Sample preparation

The $Gd_2FeCrO_6$ (GDFCO) sample was prepared through the conventional sol–gel method. High-purity chemicals, including Gadolinium Nitrate Hexahydrate ($Gd(NO_3)_3{\cdot}6H_2O$, 99.90 %), Chromium Nitrate Nonahydrate ($Cr(NO_3)_3{\cdot}9H_2O$, 99.00 %), and Iron Nitrate Nonahydrate ($Fe(NO_3)_3{\cdot}9H_2O$, 99.00 %), and were precisely measured in their stoichiometric ratios (2 mmol: 1 mmol: 1 mmol), respectively and each chemical was dissolved separately in 20 ml of de-ionized water under continuous stirring at room temperature for 30 min. All the solutions were mixed in a single beaker and stirred for an additional 30 min until a clear, transparent brown solution was obtained. Citric acid (CA) and ethylene glycol (EG) were dissolved in deionized water in separate beakers and stirred continuously for 10 min to ensure complete dissolution. Subsequently, the solutions were gradually added dropwise to the metal precursors solution, maintaining a molar ratio of 1:1:4 (metals: CA: EG). The resulting solution was stirred at 80 °C for 6 h to create a homogeneous brown gel. The gel was dried at 120 °C for 12 h to yield a brown fluffy mass in a hot air oven. The fluffy mass was homogenized into the powdered form and calcined at 800 °C for 6 h. The calcined powder was again milled and compressed into uniform cylindrical pellets of 1.5 mm thickness using hydrostatic pressure. These pellets were sintered at 1200 °C for 24 h and gradually cooled to room temperature. After sintering, the pellets were finely ground for subsequent characterization. The schematic representation of the whole synthesis process of the GDFCO compound is shown in Fig. 1.

### 2.2. Characterization

The phase purity and crystal structure of the synthesized compound were analyzed using a Rigaku Smart Lab 3 kW powder X-ray diffractometer (XRD) equipped with Cu-$K_\alpha$ radiation ($\lambda$ = 1.540 Å). Data were recorded over a $2\theta$ range of 20°-80° with a 0.02° step size, at room temperature. The structural parameters were refined using the Rietveld method with FULLPROF software. The crystal structure was built from refined results using VESTA software. Fourier transform infrared (FTIR) spectra were collected using a PerkinElmer spectrometer over the wavenumber range from 400 to 4000 $cm^{-1}$ at room temperature to analyze the functional groups and bonding characteristics. The morphological analysis of the compound was examined through the Zeiss Gemini SEM 500 field emission scanning electron microscopy (FESEM). The magnetic properties were thoroughly investigated using a vibrating sample magnetometer (VSM) (Model: J3338, Cryogenic Ltd). Magnetization versus temperature ($M-T$) data were recorded in both field cooling (FC) and zero-field cooling (ZFC) modes over the temperature range of 3–300 K, with an applied magnetic field of 100 Oe. Magnetization versus field (M−H) data were performed under a maximum applied field of ± 70 kOe in ZFC mode at different temperatures between 10–300 K. Additionally, $M-H$ isotherms were recorded in the first quadrant under the applied field of 70 kOe over the temperature

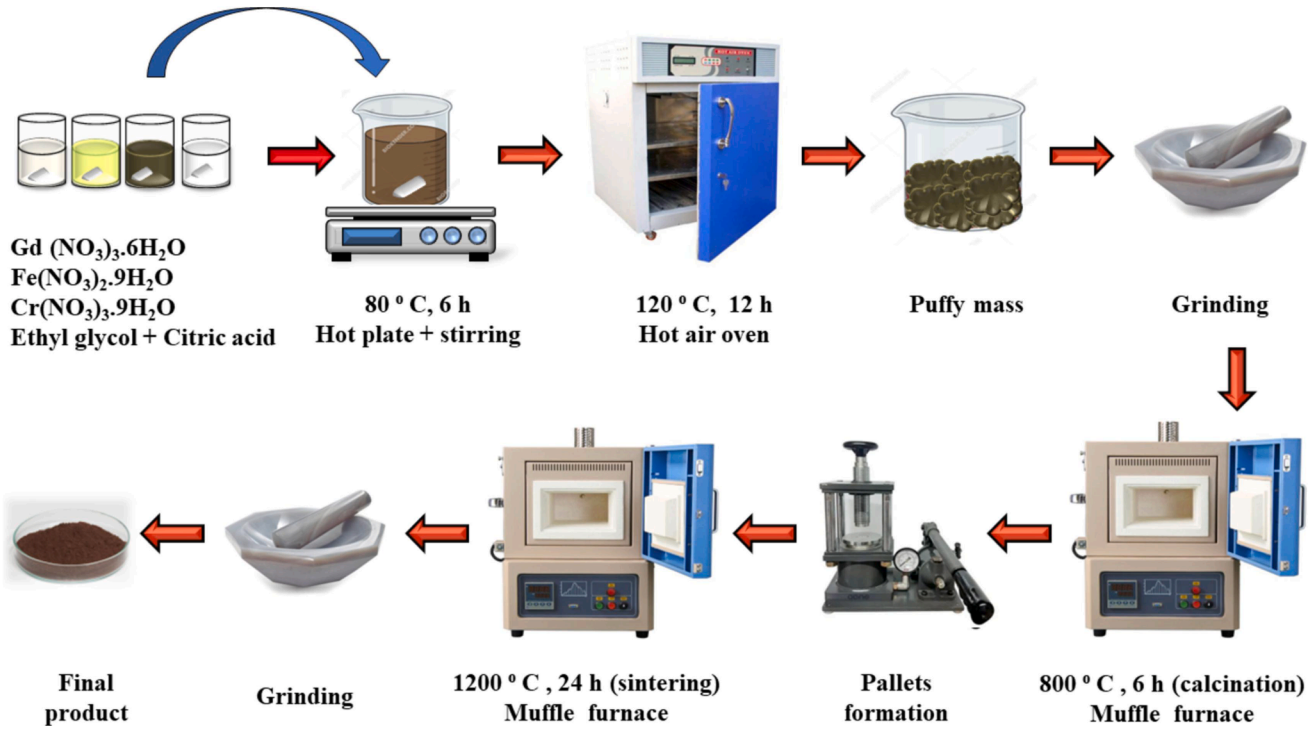


**Fig. 1.** Schematic representation of the preparation $Gd_2FeCrO_6$ (GDFCO) compound.

range of 3–30 K.

## 3. Results and discussion

### 3.1. Crystallographic structural analysis

The Rietveld-fitted XRD pattern of the $Gd_2FeCrO_6$ composition, as depicted in Fig. 2 (a), verifies the sample's phase purity. The sample contains two phases including a monoclinic with the $P2_1/n$ space group and trigonal with space group $R\,\bar{3}\,c$. However, the monoclinic was the dominating phase with 90.94 % while the trigonal phase associated with $Fe_2O_3$ was 9.06 % only. The existence of the secondary phase has been ascribed to both the local structural inhomogeneity and the martensitic type of transition. These results were consistent with previously reported findings [40,43–45]. The refinement results in terms of lattice parameters ($a$, $b$ and $c$), unit cell volume ($V$), goodness fitting parameter

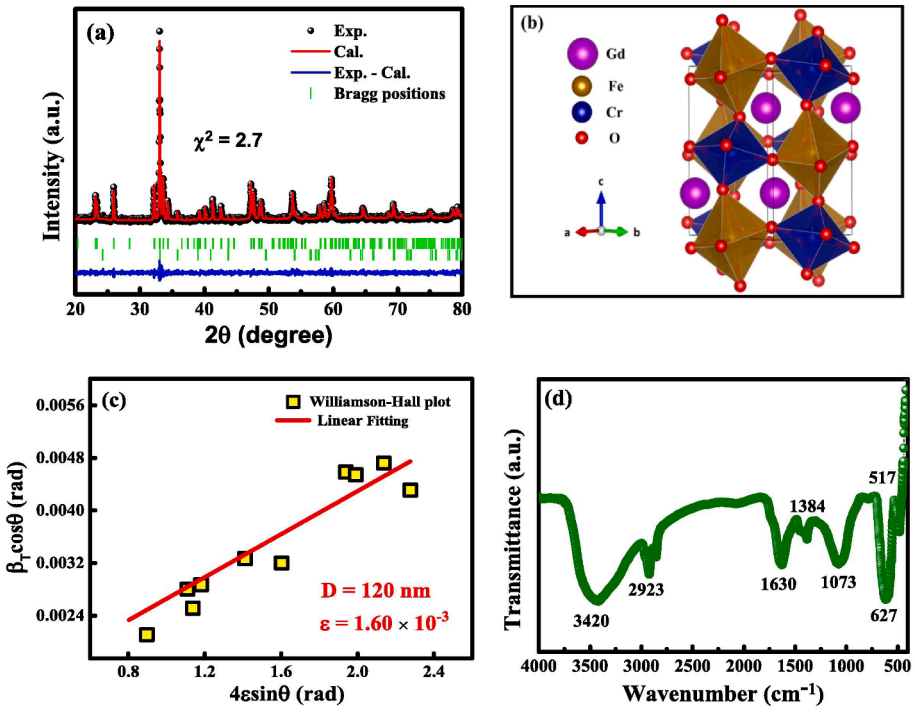


**Fig. 2.** (a) Rietveld-refined XRD pattern, (b) Schematic crystal structure using VESTA software, (c) Williamson-Hall plot, and (d) FTIR spectra of GDFCO compound.

($\chi^2$) and reliability factors for both phases, are summarized in Table 1. Moreover, based on the refined parameters, the crystal structure of GDFCO was generated using the VESTA software. The unit cell consists of corner-shared $FeO_6$ and $CrO_6$ octahedra, with Gd ions located within the voids of the octahedral framework, as illustrated in Fig. 2 (b). These cations, Fe and Cr are slightly displaced from the centers of the octahedra, contributing to the octahedral distortion. To assess the structural stability of the GDFCO compound, the Goldschmidt tolerance factor ($t_g$) [24], was calculated using the formula, $t_g = \frac{r_{Gd}+r_O}{\sqrt{2}\left(\frac{r_{Fe}+r_{Cr}}{2}\right)+r_O}$, where $r_{Gd}, r_{Fe}$, $r_{Cr}$ and $r_O$ represent the ionic radii of the $Gd^{3+}$, $Fe^{3+}$, $Cr^{3+}$ cations, and $O^{2-}$ anions, respectively [6]. The $t_g$ value for the GDFCO compound is calculated to be ~ 0.88, which emphasizes the octahedral distortion and aligns with values reported for similar perovskites [46,47].

From the XRD results, the average crystallite size ($D$) and lattice microstrain (ε) were determined using the Williamson-Hall (W-H) relation as expressed through the following equation [48,49]:

$$B_T cos\theta = \frac{K\lambda}{D} + 4\varepsilon sin\theta \quad (1)$$

Where $B_T$ represents the full width at half maximum (FWHM) of XRD peaks, $K \sim 0.94$, denotes the Debey-Scherer constant, $\lambda$ represents the wavelength of the X-ray source (0.15406 nm), and $\theta$ denotes the XRD peak position. Fig. 2 (c) illustrates the Williamson-Hall plot, from which the average crystallite size (D) and lattice microstrain ($\varepsilon$) were extracted. The calculated average values of $D$ and $\varepsilon$ are ~ 120 nm and 1.64 x$10^{-3}$, respectively. These findings are consistent with other double perovskite oxides [46].

Fig. 2 (d) demonstrates the FTIR spectrum of the GDFCO compound in a frequency range 400–4000 $cm^{-1}$. The absorption peaks ranging from 450 to 640 $cm^{-1}$ are attributed to the stretching and bending vibration of Fe/Cr-O within the $FeO_6/CrO_6$ octahedra [40,47,50]. Additionally, absorption bands near 1000–1700 $cm^{-1}$ are associated with the C = O and C–O–C stretching vibration modes [51,52], while a broad band observed between 2840–3500 $cm^{-1}$ corresponds to antisymmetric and symmetric stretching of $H_2O$ and O–H bonds due to water's surface adsorption [40,53].

### 3.2. Morphological analysis

Fig. 3 (a) exhibits the FESEM image of the GDFCO compound. It can be seen from the figure that the GDFCO compound possesses grains of irregular to nearly spherical shapes. The inset histogram in Fig. 3 (a) displays the average grain size ($G$) distribution. The average grain size of the compound was found to be ~ 281 nm using *ImageJ* Software. The EDS spectrum as display in Fig. 3 (b), confirms the presence of the desired elements *i.e.* Gd, Fe, Cr, and O in their intended proportion in the GDFCO compound. Table 2 indicates that the experimentally obtained mass and atomic percentages of these elements are well-aligned with the theoretical calculation, thereby confirming the successful synthesis of the GDFCO double perovskite.

**Table 1**
The structural and microstructural parameters for both the phases of the GDFCO compound.

| Parameters | $Gd_2FeCrO_6$ | $Fe_2O_3$ |
|---|---|---|
| *Phase fraction (%)* | *90.94* | *9.06* |
| *a* | 5.3299(1) Å | 5.0145(1) Å |
| *b* | 5.5580(1) Å | 5.0145(1) Å |
| *c* | 7.6315(2) Å | 13.864(2) Å |
| *V* | 226.07(7) Å$^3$ | 301.91(8) Å$^3$ |
| *α, γ* and *β* | 90°, 90° and 89.96 | 90°, 120° and 90° |
| $R_F$ | 6.9 | 15.7 |
| $\chi^2$ | 2.7 | |
| $t_g$ | 0.88 | |
| *D* | 120 nm | |
| ε | 1.60 x$10^{-3}$ | |
| *G* | 281 nm | |

### 3.3. Magnetic properties

The magnetic properties of the $Gd_2FeCrO_6$ (GDFCO) compound were investigated by measuring magnetization as a function of temperature (M−*T*) between 3–300 K under a 100 Oe magnetic field in both field-cooled (FC) and zero-field-cooled (ZFC) modes, as illustrated in Fig. 4. The compound exhibits two distinct magnetic transitions. The first transition occurs at $T_{N1} \sim 220$ K, marking a shift from the PM to AFM state. This transition is attributed to magnetic interactions among $Cr^{3+}$/$Fe^{3+}$ ions mediated by oxygen anions [46,47,54,55]. It is indicated by a small peak in FC mode, as highlighted in the zoomed area of the right inset in Fig. 4. However, this peak is not prominently visible in the *dM/dT* curve due to the very low magnetization in the high-temperature region that is apparently obscured by the significantly higher magnetization at lower temperatures. This transition has also been identified in the same magnetic structure-based half-doped orthochromite, specifically in the $GdFe_{0.5}Cr_{0.5}O_3$ compound [56]. As the temperature decreases further, a second magnetic phase transition is observed at $T_{N2} \sim$ 6 K, as determined by the derivative (*dM/dT*) of FC magnetization with respect to temperature, as shown in the left inset of Fig. 4. This transition corresponds to the antiferromagnetic spin order of the $Gd^{3+}$ ions [27,57]. This behaviour slightly differs from the previous findings [40,43]. A strong bifurcation emerges between the ZFC and FC curves, with the FC magnetization continuing to rise, reaching a maximum positive value at 4 K. This suggests a super-exchange interaction between the $Gd^{3+}$ spins through the $Gd^{3+}$–$O^{2-}$-$Gd^{3+}$ pathway [58].

Meanwhile, the ZFC magnetization decreases with decreasing temperature, reaching its minimum value at 4 K. This unusual negative magnetization behaviour may be accredited to the exchange interaction between the $Gd^{3+}$ ions and canted $Fe^{3+}$/$Cr^{3+}$ spins. This phenomenon has also been observed in other similar perovskite compounds [46,59,60].

To enhance a better insight into the magnetic ordering in the present GDFCO compound, isothermal magnetization loops were recorded as a function of the applied field within the range of ± 70 kOe at various temperatures (10 K, 20 K, 30 K, 100 K and 300 K), as illustrated in Fig. 5. The loops exhibit a clear hysteresis in the low magnetic field region, below $T_{N1}$, as shown in the upper inset of Fig. 5. As the temperature increases, the hysteresis loops become narrower, and above $T_{N1}$, loops disappear at 300 K, indicating a transition to the paramagnetic PM state. Additionally, the hysteresis loops remain unsaturated (symmetrically closed) even at ± 70 kOe magnetic fields, suggesting the presence of both high-field antiferromagnetism and low-field weak ferromagnetism, likely resulting from antisymmetric Dzyaloshinskii-Moriya (DM) interactions.

The contribution of these mixed states can be described by the relation $M(H) = \chi_{AFM}H + M_S$, where the first term ($\chi_{AFM}$) represents the antiferromagnetic (AFM) contribution, and the second term ($M_S$) denotes the magnetization saturation. To determine $M_S$ at different temperatures, the high-filed linear AFM contribution is subtracted from the total magnetization. The lower inset of Fig. 5 illustrates the changes in the coercive field ($H_C$) and magnetization saturation ($M_S$) as a function of temperature, which consistently decrease as the temperature increases, and above $T_{N1}$, both parameters drop to zero, indicating the onset of the paramagnetic phase in the GDFCO compound.

### 3.4. Magnetocaloric properties

To further investigate the nature of the magnetic transition at $T_{N2}$ and examine the magnetocaloric (MC) properties of the GDFCO compound, isothermal magnetization curves were measured in the first quadrant at various temperatures from 3 K to 30 K, with the applied magnetic field varying from 0 to 70 kOe, as shown in Fig. 6 (a). The

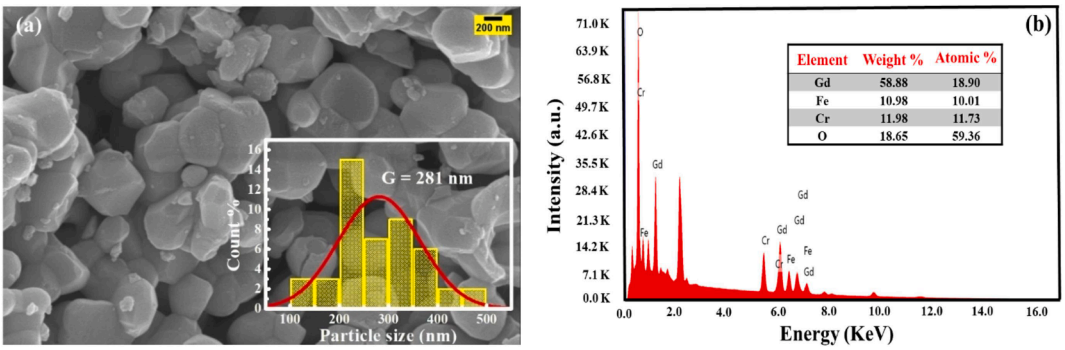


**Fig. 3.** (a) FESEM micrographs and inset show the histogram of average grain size distribution, and (b) EDS spectra of GDFCO compound.

**Table 2**
The experimentally and theoretically calculated mass and atomic counts of different elements in the GDFCO compound.

| Elements | Theoretically Mass of Elements (%) | Experimentally Mass of Elements (%) | Theoretically Atomic Count of Elements (%) | Experimentally Atomic Count of Elements (%) |
|---|---|---|---|---|
| **Gd** | 60.67 | 58.88 | 20 | 18.90 |
| **Fe** | 10.77 | 10.98 | 10 | 10.01 |
| **Cr** | 10.03 | 11.98 | 10 | 11.73 |
| **O** | 18.52 | 18.65 | 60 | 59.36 |
| **Total** | 100 | 100 | 100 | 100 |

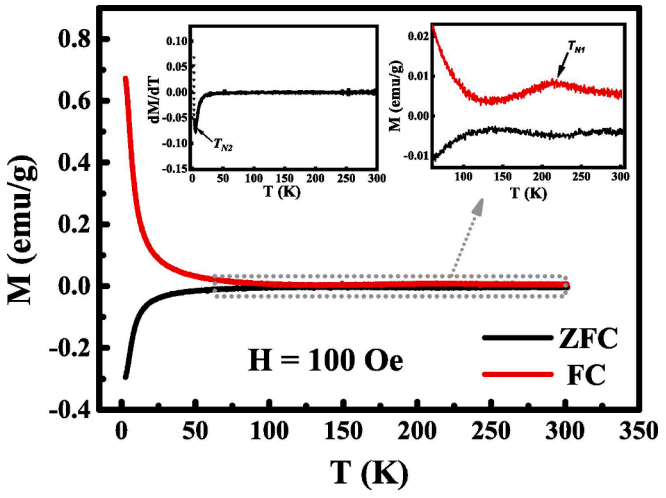


**Fig. 4.** Temperature-dependent magnetization ($M-T$) data in both FC and ZFC modes at an applied magnetic field of 100 Oe between 3 K to 300 K. The left inset displays the $dM/dT$ vs. $T$ in FC mode, while the right inset shows the zoomed-in view of M−T curve for the GDFCO compound.

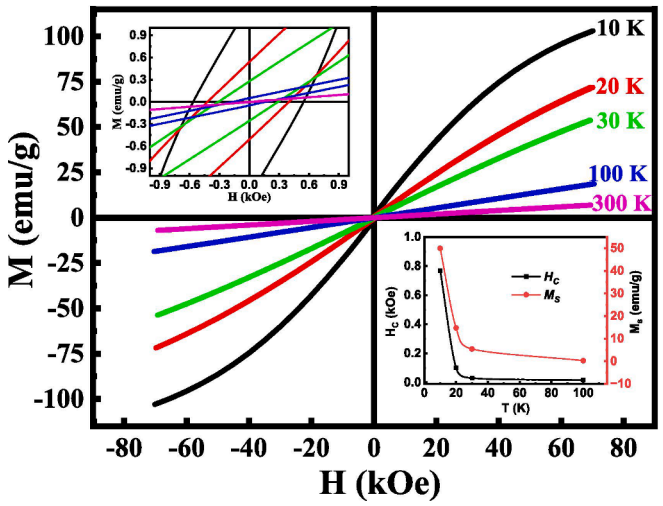


**Fig. 5.** Field-dependent magnetization ($M-H$) data at various temperatures from 10 K to 300 K with an applied magnetic field up to ± 70 kOe. The upper inset displays the enlarged view of hysteresis loops, while the lower inset shows the coercive field ($H_C$) and saturation magnetization ($M_S$) variation with the temperature of the GDFCO compound.

magnetocaloric effect is typically associated with magnetic transitions and is significantly affected by the nature of these magnetic transition [7,61]. To ascertain the characteristics of the magnetic phase transition at $T_{N2}$ in the GDFCO compound, the Banerjee criterion was employed. According to this, Arrott's plot ($H/M$ vs. $M^2$) displays a negative slope for first-order phase transition (FOPT) and a positive slope indicates second-order phase transition (SOPT) [62,63]. Arrott's plots for the GDFCO compound, illustrated in Fig. 6 (b), clearly show a positive slope, indicating a second-order magnetic phase transition (SOMT). Materials exhibiting second-order magnetic phase transitions (SOPT) with a significant magnetocaloric effect (MCE) are preferred for magnetic refrigeration. Their ability to provide substantial magnetic cooling capacity across a wide temperature range makes them ideal candidates for efficient magnetic refrigeration applications [63,64].

The magnetocaloric effect of the GDFCO compound can be examined in terms of magnetic entropy change ($\Delta S_M$) and the relative cooling power ($RCP$). These parameters are critical for evaluating the magnetic refrigeration capacity and its cooling efficiency, respectively. The magnetic entropy change ($\Delta S$) can be determined using the Maxwell's thermodynamic relations [65].

$$\Delta S(T)_{\Delta H} = \int_{HI}^{HF} \left(\frac{\partial M(T,H)}{\partial T}\right) dH \tag{2}$$

The numerical integration of equation (2), using the Trapezoidal rule is given by [66]:

$$\Delta S(T_{av})_{\Delta H} = \frac{\delta H}{2\delta T}\left(\delta M_1 + 2\sum_{i=2}^{n-1}\delta M_i + \delta M_n\right) \tag{3}$$

Here, the average temperature, $T_{av}$ is calculated as $[(T_j + T_{j+1})/2)]$, where $T_j$ and $T_{j+1}$ are two consecutive temperatures corresponding to

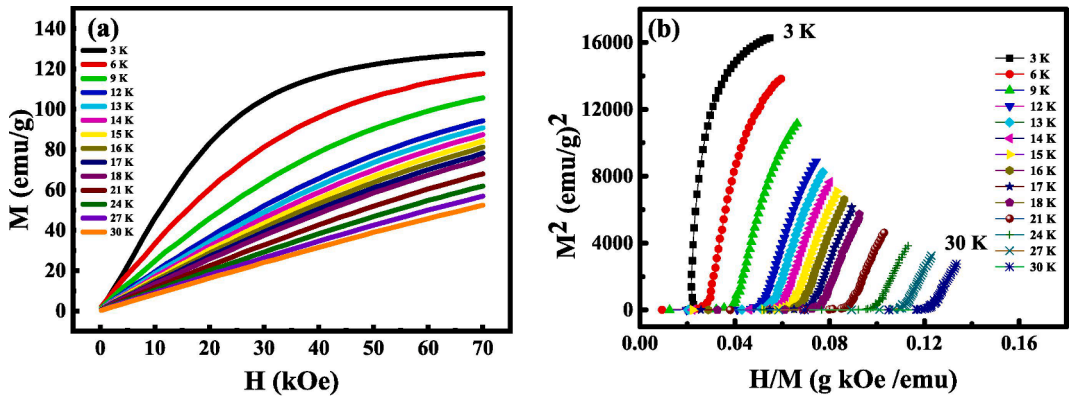


**Fig. 6.** (a) Selected $M(H)$ curves in the 1st quadrant from 10 K to 300 K with an applied magnetic field up to 70 kOe (b) Arott plot ($M^2$ versus $H/M$) between 3 K to 30 K for GDFCO compound.

magnetization isotherms with a change in the magnetic field by $\Delta H = H_F - H_I$ with a uniform step size $\delta H$. The difference in temperature between the two isotherms is represented by $\delta T = T_{j+1} - T_j$. For each of the two isotherms, n points are measured as the magnetic field varies from $H_1 = H_I$ to $H_n = H_F$ at a step size of $\delta H = \Delta H / (n-1)$. Additionally, the change in magnetization between $T_j$ and $T_{j+1}$ for each magnetic field step, ranging from 1 to $n$ represented by $\delta M_i = [M(T_{j+1})_I - M(T_j)_i]$. The sign of $-\Delta S$ provides information on the magnetic transition type; it is positive for a ferromagnetic transition and negative for an antiferromagnetic transition. Fig. 7 (a) shows the variation of entropy change ($-\Delta S$) with temperature across various magnetic fields. The graph exhibits that $-\Delta S$ remains positive over the entire temperature range, reaching a peak value of $-\Delta S_M \sim 38.6$J/kg K at 70 kOe. This value significantly exceeds those reported for other rare earth double perovskite compounds [11,29,36,67–70]. Several factors contribute to this significant MCE such as the compound's higher magnetization and lower coercive fields, which reduce energy loss during thermal processes and result in a higher change in magnetic entropy ($-\Delta S$) values. Additionally, the magnetic interaction between $Gd^{3+}$ ions near their magnetic ordering temperature (around 4.5 K) further enhances the ($-\Delta S$) values. The alignment of the orbital and spin moments of Gd ions with the Fe-Cr sublattice contributes to the large rare earth moments of the heavier $Gd^{3+}$ ions,

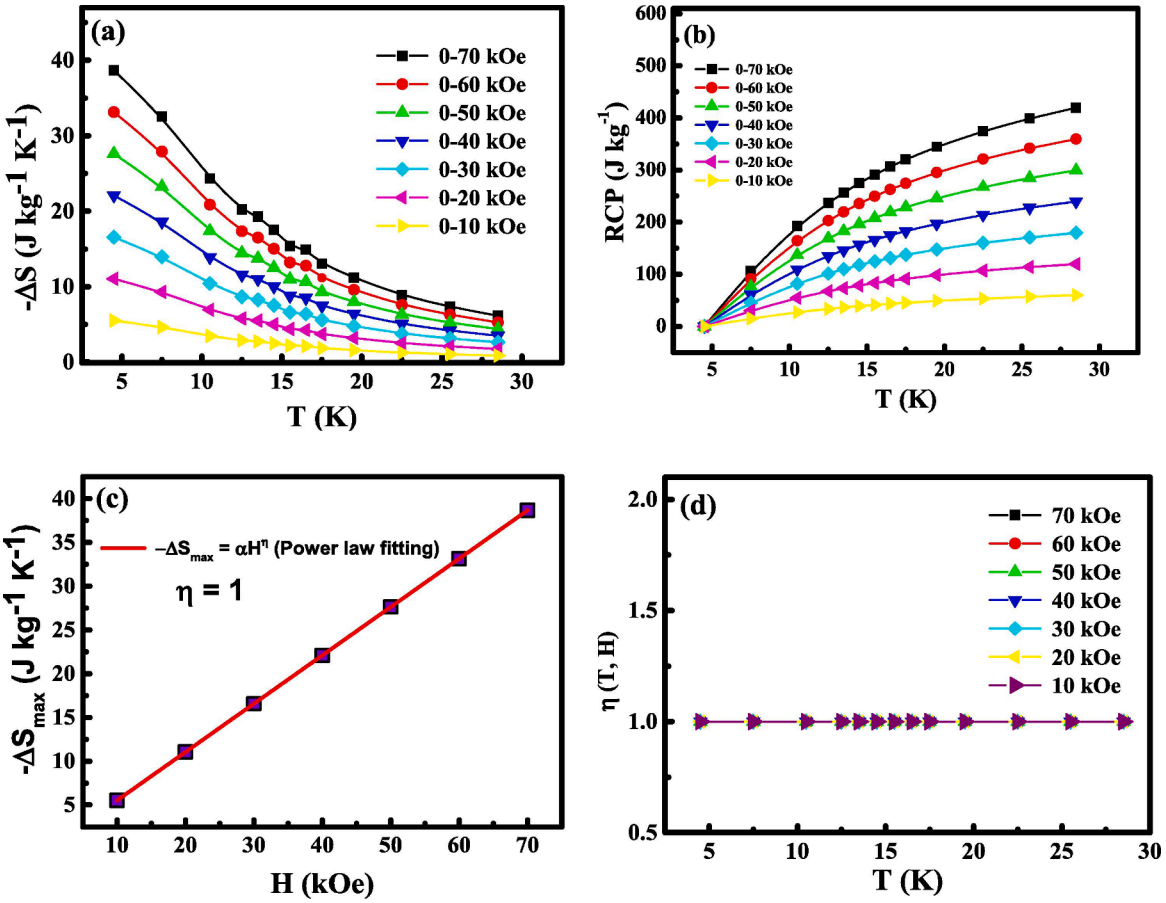


**Fig. 7.** (a) The change in magnetic entropy ($-\Delta S_M$), as a function of temperature, (b) variation of *RCP* with temperature between 3 K to 30 K with an applied magnetic field up to 70 kOe, (c) The values of maximum change in entropy ($-\Delta S_{max}$) versus applied field fitted by relation $-\Delta S_{max} = \alpha H^{\eta}$ and (d) temperature dependence of $\eta(T, H)$ at different magnetic fields for GDFCO compound.

**Table 3**
Comparison of MCE parameters such as maximum magnetic entropy change ($-\Delta S_M$), relative cooling power (RCP), magnetic transition temperature ($T_M$) and applied magnetic field range ($\Delta H$) for GDFCO compound and other recently reported rare-earth-based oxides.

| Materials | $-\Delta S_M$ (J/kg K) | *RCP* (J/kg) | $T_M$ (K) | $\Delta H$ (kOe) | References |
|---|---|---|---|---|---|
| **$Gd_2FeCrO_6$** | **27.61** | **299.5** | **4.5** | **0–50** | **Present** |
| | **38.60** | **418** | | **0–70** | **work** |
| $Gd_2ZnMnO_6$ | 15.17 | 226.2 | 6.4 | 0–50 | [18] |
| $Ho_2ZnMnO_6$ | 13.19 | 246.5 | 6.8 | | |
| $Gd_2FeCoO_6$ | 21.57 | 346.1 | 4.9 | 0–70 | [68] |
| $Er_2FeCoO_6$ | 14.60 | 280.7 | 2.7 | | |
| $Gd_2CuMnO_6$ | 7.84 | 151.1 | 7.5 | 0–50 | [76] |
| $Dy_2CuMnO_6$ | 5.69 | 180.9 | 12.1 | | |
| $Gd_2NiMnO_6$ | 35.5 | – | 2 | 0–70 | [29] |
| $Er_2CrMnO_6$ | 12.94 | 277.5 | 5.2 | 0–70 | [26] |
| $Ho_2CrMnO_6$ | 11.03 | 322.7 | 6.1 | | |
| $Pr_2FeCrO_6$ | 2.06 | – | 14 | 0–90 | [46] |
| $Dy_2FeCrO_6$ | 12.64 | 241.1 | 15.5 | 0–50 | [11] |
| $Tb_2FeCrO_6$ | 12.9 | 341.4 | 8.5 | 0–70 | [39] |
| $Er_2FeCrO_6$ | 11.95 | 215.8 | 11.7 | 0–50 | [36] |
| $Tm_2FeCrO_6$ | 4.78 | 123.6 | 10.5 | | |

resulting in a positive change in entropy during magnetocaloric effect measurements at low temperatures [25,28,70]. These factors suggest that the compound has promising potential for magnetic refrigeration applications.

Moreover, the relative cooling power (*RCP*), serves as a metric for assessing the efficiency of magnetic refrigeration and the material's potential for magnetic cooling applications. It quantifies the heat transfer in an ideal magnetic refrigeration cycle from a warm reservoir to a cold reservoir and is determined by the following expression:

$$RCP = \int_{T_1}^{T_2} \Delta S(T_{av})_{\Delta H} dT \tag{4}$$

Where $T_1$ and $T_2$ represent the magnetic refrigeration cycle's lower and higher temperatures respectively. The calculated *RCP* values at different applied magnetic fields are shown in Fig. 7 (b). The maximum *RCP* observed is $\sim$ 418 J $kg^{-1}$ at 70 kOe. Table 3 provides a comparison of magnetocaloric parameters, including $-\Delta S_M$, *RCP* and $T_M$ values for our GDFCO compound and other recently studied rare-earth based double perovskites. The comparison demonstrates that Gd-doped compounds, particularly GDFCO, exhibit superior magnetocaloric properties compared to other rare-earth doped double perovskites. GDFCO shows the highest value $-\Delta S_M = 27.61$ J/kg K and an *RCP* of 299.5 J/kg at 0–50 kOe, significantly exceeding the values reported for other compounds Additionally, compounds in the $R_2FeCrO_6$ family generally show lower $-\Delta S_M$ and *RCP* values when compared with those for $Gd_2FeCrO_6$ compound, further emphasizing the exceptional magnetocaloric performance of the $Gd_2FeCrO_6$ compound in the present study. These results suggest that $Gd_2FeCrO_6$ is a highly promising candidate for magnetic refrigeration applications, offering enhanced efficiency and performance compared to other materials.

For materials exhibiting a SOPT, the field dependence of the maximum magnetic entropy change ($\Delta S_{max}$) is expected to follow a power-law relationship, expressed as [71,72]:

$$-\Delta S_{max} = aH^{\eta} \tag{5}$$

Here, $a$ represents a constant, and the exponent η is indicative of the magnetic order of the material. Fig. 7 (c) presents the power law fitting of the experimental data ($\Delta S_{max}$ versus $H$) yielded a value of $\eta = 1$, suggesting that the power law exponent aligns with the expected behaviour. Moreover, the value of $\eta$ was calculated using the given expression [73].

$$\eta = \frac{dln|-\Delta S_{max}|}{dlnH} \tag{6}$$

Fig. 7 (d), illustrates the temperature dependence of $\eta$ across different magnetic field strengths. Remarkably, $\eta$ consistently equals 1 over the entire temperature range, aligning with other compounds [74]. This value exceeds the commonly reported $\eta = 0.67$ for ferromagnetic materials governed by mean-field theory [72]. The high value of $\eta$ suggests the existence of antiferromagnetic interactions in the ferromagnetic matrix [74–76]. However, if the value of $\eta$ exceeds 2, it corresponds to the first-order phase transition (FOPT) [72]. Thus, the value of $\eta = 1$, in this case, confirms that the material exhibits second-order magnetic behaviour with possible mixed magnetic interactions, including antiferromagnetic correlations.

## 4. Conclusions

In summary, the $Gd_2FeCrO_6$ (GDFCO) was synthesized using the conventional sol–gel route. XRD refinement confirmed the predominantly monoclinic ($P2_1/n$) crystal structure with a minor secondary trigonal phase ($R\,\overline{3}\,c$). The FESEM micrograph displayed a homogeneous grain distribution with well-defined grain boundaries. The EDS spectrum verified the existence of required elements *i.e.* Gd, Fe, Cr, and O as per their stoichiometric proportion in the GDFCO compound. The compound shows the second-order phase transition (SOPT). The magnetocaloric effect, characterized by the change in entropy ($-\Delta S_M$) and relative cooling power (*RCP*) under a varying field of 0–70 kOe achieved $\sim$ 38.6 J/kg K and $\sim$ 418 J/kg, respectively. These properties make the $Gd_2FeCrO_6$ compound a promising applicant for magnetocaloric effect (MCE) based magnetic refrigeration applications, particularly at cryogenic temperatures.

## CRediT authorship contribution statement

**Meenakshi:** Original manuscript writing, Review and editing, Conceptualization, Visualization, Formal analysis, Data curation. **Sanjay Saini:** Writing – review & editing, Formal analysis, Validation, Data curation. **Neeraj Panwar:** Writing – review & editing, Visualization, Validation, Formal analysis. **Ramovatar:** Writing – review & editing, Visualization, Validation, Software, Formal analysis, Conceptualization, Supervision. **Surendra Kumar:** Writing – review & editing, Visualization, Validation, Software, Formal analysis, Conceptualization.

## Declaration of competing interest

The authors declare that they have no known competing financial interests or personal relationships that could have appeared to influence the work reported in this paper.

## Acknowledgment

The authors express sincere gratitude to the Central Instrumentation Laboratory, Guru Jambheshwar University, Hisar and University Science Instrumentation Centre, University of Delhi, New Delhi for providing the XRD and FESEM facilities, respectively. One of the authors Ms. Meenakshi extends her gratitude to the Central University of Haryana (CUH) for granting the University Research Fellowship (URF).

## Data availability

Data will be made available on request.

## References

[1] L. Li, M. Yan, Recent progresses in exploring the rare earth based intermetallic compounds for cryogenic magnetic refrigeration, J. Alloys Compd. 823 (2020) 153810.
[2] M. Balli, S. Jandl, P. Fournier, A. Kedous-Lebouc, Advanced materials for magnetic cooling: Fundamentals and practical aspects, Appl. Phys. Rev. 4 (2017) 021305.

[3] I.A. Abdel-Latif, M.R. Ahmed, Use of Magnetocaloric Material for Magnetic Refrigeration System: A Review, Mater. Sci. Res. India. 16 (2019) 209–224.
[4] V. Franco, J.S. Blázquez, J.J. Ipus, J.Y. Law, A. Conde, Progress in Materials Science Magnetocaloric effect : From materials research to refrigeration devices, Prog. Mater. Sci. 93 (2018) 112–232.
[5] T. Gottschall, K.P. Skokov, M. Fries, A. Taubel, I. Radulov, F. Scheibel, D. Benke, S. Riegg, O. Gutfleisch, Making a Cool Choice : The Materials Library of Magnetic Refrigeration, Adv. Energy Mater. 1901322 (2019) 1–13.
[6] M.A. Peña, J.L.G. Fierro, Chemical structures and performance of perovskite oxides, Chem. Rev. 101 (2001) 1981–2017.
[7] W. Zhong, C.T. Au, Y.W. Du, Review of magnetocaloric effect in perovskite-type oxides, Chinese Phys. b. 22 (2013) 057501.
[8] M.H. Phan, S.C. Yu, Review of the magnetocaloric effect in manganite materials, J. Magn. Magn. Mater. 308 (2007) 325–340.
[9] L. Fu, B. Li, S. Li, L. Yin, Magnetic, Electronic, and Optical Properties of Perovskite Materials, Mater. Horiz. (2020) 43–59.
[10] A. Barman, S. Kar-Narayan, D. Mukherjee, Caloric Effects in Perovskite Oxides, Adv. Mater. Interfaces. 6 (2019) 1–31.
[11] C. Agarwal, H. Mittal, T. Bano, J. Kumar, M. Gora, A. Kumar, A Review on Recent Advancements in Rare-Earth based Double Perovskite Compounds, J. Pure Appl. Phys. 10 (2022) 1–16.
[12] X.M. Chen, L. Bellaiche, tunable ferromagnetic and electrical properties, Nat. Commun. 4021 (2014) 1–7.
[13] M. Le, P. Gr, High-temperature multiferroicity and strong magnetocrystalline anisotropy in 3d–5d double perovskites, Phys. Rev. b. 83 (2011) 024410.
[14] T. Cai, S. Liu, S. Ju, C. Liu, G. Guo, Photovoltaics and Spintronics, Phys. Rev. Appl. 8 (2017) 034034.
[15] K. Aswathi, J. Pezhumkattil Palakkal, R. Revathy, M.R. Varma, Sign reversal of magnetization in $Sm_2CrMnO_6$ perovskites, J. Magn. Magn. Mater. 483 (2019) 89–94.
[16] P. Nimno, P. Comno, Y. Zhang, H. Li, D. Guo, L. Hou, X. Li, Z. Ren, G. Wilde, Cryogenic magnetic properties and magnetocaloric performance in double perovskite $Pr_2NiMnO_6$ and $Pr_2CoMnO_6$ compounds, Ceram. Int. 44 (2018) 20762–20767.
[17] L. Li, P. Xu, S. Ye, Y. Li, G. Liu, D. Huo, M. Yan, Magnetic properties and excellent cryogenic magnetocaloric performances in B-site ordered $RE_2ZnMnO_6$ (RE = Gd, Dy and Ho) perovskites, Acta Mater. 194 (2020) 354–365.
[18] J.Y. Moon, M.K. Kim, Y.J. Choi, N. Lee, Giant Anisotropic Magnetocaloric Effect in Double-perovskite $Gd_2CoMnO_6$ Single Crystals, Sci. Rep. 16099 (2017) 1–10.
[19] K. Yao, Y. Xu, Magnetic Properties and Cryogenic Magneto-caloric Effect (MCE) in the $Dy_2FeCrO_6$ Oxide Compound, J. Supercond. Nov. Magn. 35 (2022) 1307–1311.
[20] S. Vasala, M. Karppinen, $A_2B'B''O_6$ perovskites: A review, Prog. Solid State Chem. 43 (2015) 1–36.
[21] A. Hossain, P. Bandyopadhyay, S. Roy, An overview of double perovskites $A_2B'B''O_6$ with small ions at A site: Synthesis, structure and magnetic properties, J. Alloys Compd. 740 (2018) 414–427.
[22] L. Li, M. Yan, Recent progress in the development of $RE_2TMTM'O_6$ double perovskite oxides for cryogenic magnetic refrigeration, J. Mater. Sci. Technol. 136 (2023) 1–12.
[23] T. Saha-Dasgupta, Double perovskites with 3d and 4d/5d transition metals: Compounds with promises, Mater. Res. Express. 7 (2019) 014003.
[24] M.T. Anderson, K.B. Greenwood, G.A. Taylor, K.R. Poeppelmeier, B-cation arrangements in double perovskites, Prog. Solid State Chem. 22 (1993) 197–233.
[25] Q. Wang, B. Lv, Q. Wu, X. Hu, X. Luo, J. Fang, N. Yu, H. Yang, M. Pan, H. Ge, Study on the critical behavior and magnetocaloric effect of $RCrO_3$ (R = Gd, Dy), Ceram. Int. 49 (2023) 11903–11911.
[26] B. Wu, D. Guo, Y. Wang, Y. Zhang, Crystal structure, magnetic properties, and magnetocaloric effect in B-site disordered $RE_2CrMnO_6$ (RE = Ho and Er) perovskites, Ceram. Int. 46 (2020) 11988–11993.
[27] A. Prusty, S. Mahana, A. Gloskovskii, D. Topwal, U. Manju, Gd induced modifications in the magnetocaloric properties of dysprosium manganites, J. Alloys Compd. 883 (2021) 160862.
[28] J. Shi, S. Yin, M.S. Seehra, M. Jain, Enhancement in magnetocaloric properties of $ErCrO_3$ via A-site Gd substitution, J. Appl. Phys. 123 (2018).
[29] J.K. Murthy, K.D. Chandrasekhar, S. Mahana, D. Topwal, Giant magnetocaloric effect in $Gd_2NiMnO_6$ and $Gd_2CoMnO_6$ ferromagnetic insulators, J. Phys. d: Appl. Phys. 48 (2015) 355001.
[30] K. Miura, K. Terakura, Electronic and magnetic properties of $La_2FeCrO_6$: Superexchange interaction for a $d^5$–$d^3$ system, Phys. Rev. B - Condens. Matter Mater. Phys. 63 (2001) 7.
[31] H. Wu, Z. Pei, W. Xia, Y. Lu, K. Leng, X. Zhu, Structural, magnetic, dielectric and optical properties of double-perovskite $Bi_2FeCrO_6$ ceramics synthesized under high pressure, J. Alloys Compd. 819 (2020) 153007.
[32] J.B. Goodenough, Theory of the role of covalence in the perovskite-type manganites $LaMnO_3$, Phys. Rev. 100 (1955) 564.
[33] J. Kanamori, Superexchange interaction and symmetry properties of electron orbitals, J. Phys. Chem. Solids. 10 (1959) 87–98.
[34] P. Baettig, C. Ederer, N.A. Spaldin, First principles study of the multiferroics $BiFeO_3$, $Bi_2FeCrO_6$, and $BiCrO_3$: Structure, polarization, and magnetic ordering temperature, Phys. Rev. B - Condens. Matter Mater. Phys. 72 (2005) 1–8.
[35] S. Ravi, Multiferroism in $Pr_2FeCrO_6$ perovskite, J. Rare Earths. 36 (2018) 1175–1178.
[36] Z. Dong, Z. Wang, S. Yin, Structural, magnetic and cryogenic magneto-caloric properties in $RE_2FeCrO_6$ (RE = Er and Tm) compounds, Ceram. Int. 46 (2020) 26632–26636.
[37] R.P. Maiti, S. Dutta, M.K. Mitra, D. Chakravorty, Large magnetodielectric effect in nanocrystalline double perovskite $Y_2FeCrO_6$, J. Phys. d. Appl. Phys. 46 (2013) 415303.
[38] K.P. Patra, S. Ravi, Sign reversal of both spontaneous and conventional exchange bias in nanoparticles of $Y_2FeCrO_6$ double perovskite, J. Appl. Phys. 132 (2022) 213903.
[39] S. Huang, J. Lin, Y. Shu, Y. Zhang, Magnetic Properties and Magnetocaloric Effect in $Tb_2FeCrO_6$ Double Perovskite Oxide, J. Electron. Mater. 53 (2024) 2302–2308.
[40] M.D.I. Bhuyan, S. Das, M.A. Basith, Sol-gel synthesized double perovskite $Gd_2FeCrO_6$ nanoparticles: Structural, magnetic and optical properties, J. Alloys Compd. 878 (2021) 2–11.
[41] M.D.I. Bhuyan, R. Hossain, F. Ara, M.A. Basith, A first-principles study on the phase stability and physical properties of a B-site ordered $Nd_2CrFeO_6$ double perovskite, Phys. Chem. Chem. Phys. 24 (2022) 1569–1579.
[42] S. Das, M.D.I. Bhuyan, M.A. Basith, First-principles calculation of the electronic and optical properties of $Gd_2FeCrO_6$ double perovskite: Effect of Hubbard U parameter, J. Mater. Res. Technol. 13 (2021) 2408–2418.
[43] S. Kumawat, D.K. Meena, M. Rani, H.S. Anuradha, G.A. Mund, Effect of Mg doping at Fe/Cr site on magnetic and optical properties of $Gd_2FeCrO_6$ double perovskite, J. Alloys Compd. 978 (2024) 173339.
[44] C. Gökhan Ünlü, M. Burak Kaynar, T. Şimşek, A. Tekgül, B. Kalkan, Ş. Özcan, Structure and magnetic properties of $(La_{1-x}Fe_x)FeO_3$ (x = 0, 0.25, 0.50) perovskite, J. Alloys Compd. 784 (2019) 1198–1204.
[45] C. Casut, I. Malaescu, C.N. Marin, M. Miclau, The Effect of $Bi_2O_3$ and $Fe_2O_3$ Impurity Phases in $BiFeO_3$ Perovskite Materials on Some Electrical Properties in the Low-Frequency Field, Materials (basel). 15 (2022) 4764.
[46] D. Mazumdar, I. Das, Structural, magnetic, and magnetocaloric properties of the multiferroic host double perovskite compound $Pr_2FeCrO_6$, Phys. Chem. Chem. Phys. 23 (2021) 5596–5606.
[47] M.A. Islam, T. Sato, F. Ara, M.A. Basith, Sol-gel based synthesis to explore structure, magnetic and optical properties of double perovskite $Y_2FeCrO_6$ nanoparticles, J. Alloys Compd. 944 (2023) 169066.
[48] G.K. Williamson, W.H. Hall, X-ray line broadening from filed aluminium and wolfram, Acta Metall. 1 (1953) 22–31.
[49] V. Biju, N. Sugathan, V. Vrinda, S.L. Salini, Estimation of lattice strain in nanocrystalline silver from X-ray diffraction line broadening, J. Mater. Sci. 43 (2008) 1175–1179.
[50] V.M. Gaikwad, M. Brahma, R. Borah, S. Ravi, Structural, optical and magnetic properties of $Pr_2FeCrO_6$ nanoparticles, J. Solid State Chem. 278 (2019) 120903.
[51] N. Zarrin, S. Husain, W. Khan, S. Manzoor, Sol-gel derived cobalt doped $LaCrO_3$: Structure and physical properties, J. Alloys Compd. 784 (2019) 541–555.
[52] R. Mguedla, A. Ben Jazia Kharrat, S. Kammoun, K. Khirouni, W. Boujelben, Optical studies of multiferroic $HoCrO_3$ perovskite compound for optoelectronic device applications, Opt. Mater. (amst). 119 (2021) 111311.
[53] M.N. Siddique, M. Faizan, S. Riyajuddin, P. Tripathi, S. Ahmad, K. Ghosh, Intrinsic structural distortion assisted optical and magnetic properties of orthorhombic rare-earth perovskite $La_{1-x}Eu_xCrO_3$: Effect of t-e hybridization, J. Alloys Compd. 850 (2021) 156748.
[54] K.D. Singh, F. Singh, R.J. Choudhary, R. Kumar, Consequences of $R^{3+}$ cationic radii on the dielectric and magnetic behavior of $RCrO_3$ perovskites, Appl. Phys. A Mater. Sci. Process. 126 (2020) 1–8.
[55] N. Panwar, K. Singh, K. Kanwar, Y. Bitla, S. Kumar, V.S. Puli, Low-Temperature Magnetic and Magnetocaloric Properties of Manganese-Substituted $Gd_{0.5}Er_{0.5}CrO_3$ Orthochromites, Crystals. 12 (2022) 15–20.
[56] B.B. Dash, S. Ravi, Structural, magnetic and electrical properties of Fe substituted $GdCrO_3$, Solid State Sci. 83 (2018) 192–200.
[57] M. Wang, R. Wang, H. Dai, T. Li, Y. Sun, D. Liu, F. Yan, T. Ping, A comparative study of the structure, defects, optical, dielectric, and magnetic properties of $GdMnO_3$ multiferroic ceramics synthesized by solid-state reaction and sol-gel methods, Ceram. Int. 48 (2022) 21663–21671.
[58] P. Gupta, R. Bhargava, R. Das, P. Poddar, Static and dynamic magnetic properties and effect of surface chemistry on the morphology and crystallinity of $DyCrO_3$ nanoplatelets, RSC Adv. 3 (2013) 26427–26432.
[59] S. Kumar, I. Coondoo, A. Rao, B.H. Lu, Y.K. Kuo, A.L. Kholkin, N. Panwar, Impact of low level praseodymium substitution on the magnetic properties of $YCrO_3$ orthochromites, Phys. B Condens. Matter. 510 (2017) 104–108.
[60] Y. Su, J. Zhang, Z. Feng, Z. Li, Y. Shen, S. Cao, Magnetic properties of rare earth $HoCrO_3$ chromites, J. Rare Earths. 29 (2011) 1060–1065.
[61] V. Franco, J.S. Blázquez, J.J. Ipus, J.Y. Law, L.M. Moreno-Ramírez, A. Conde, Magnetocaloric effect: From materials research to refrigeration devices, Prog. Mater. Sci. 93 (2018) 112–232.
[62] B.K. Banerjee, On a generalised approach to first and second order magnetic transitions, Phys. Lett. 12 (1964) 16–17.
[63] G. Singh, A. Gaur, P. Bisht, R.N. Mahato, Effect of bismuth doping on structural, morphological, Griffiths-like phase, and magnetocaloric properties in $La_{0.9-x}Bi_xBa_{0.1}MnO_3$ (x = 0, 0.05, and 0.1), J. Magn. Magn. Mater. 591 (2024) 171731.
[64] T. Guo, Y. Hu, X. Wang, Y. Cui, W. Li, X. Zhao, Magnetocaloric properties of double-perovskite $Sr_{1.98}Al_{0.02}FeMoO_6$, Ceram. Int. 44 (2018) 20380–20385.
[65] A.M. Tishin, Magnetocaloric effect in the vicinity of magnetic phase transition, J. Magn. Magn. Mater. 184 (1998) 62–66.
[66] V.K. Pecharsky, K.A. Gschneidner, Magnetocaloric effect from indirect measurements: Magnetization and heat capacity, J. Appl. Phys. 86 (1999) 565–575.

[67] B. Wu, Y. Zhang, D. Guo, J. Wang, Z. Ren, Structure, magnetic properties and cryogenic magneto-caloric effect (MCE) in $RE_2FeAlO_6$ (RE = Gd, Dy, Ho) oxides, Ceram. Int. 47 (2021) 6290–6297.
[68] Z. Dong, S. Yin, Structural, magnetic and magnetocaloric properties in perovskite $RE_2FeCoO_6$ (RE = Er and Gd) compounds, Ceram. Int. 46 (2020) 1099–1103.
[69] R.X. Silva, R.M. Almeida, R.L. Moreira, R. Paniago, M.V.S. Rezende, C.W. A. Paschoal, Vibrational properties and infrared dielectric features of $Gd_2CoMnO_6$ and $Y_2CoMnO_6$ double perovskites, Ceram. Int. 45 (2019) 4756–4762.
[70] S. Yin, M. Jain, Enhancement in magnetocaloric properties of holmium chromite by gadolinium substitution, J. Appl. Phys. 120 (2016) 043906.
[71] H. Oesterreicher, F.T. Parker, Magnetic cooling near Curie temperatures above 300 K, J. Appl. Phys. 55 (1984) 4334–4338.
[72] K.P. Shinde, E.J. Lee, M. Manawan, A. Lee, S.Y. Park, Y. Jo, K. Ku, J.M. Kim, J. S. Park, Structural, magnetic, and magnetocaloric properties of $R_2NiMnO_6$ (R = Eu, Gd, Tb), Sci. Rep. 11 (2021) 1–12.
[73] V. Franco, A. Conde, Scaling laws for the magnetocaloric effect in second order phase transitions: From physics to applications for the characterization of materials, Int. J. Refrig. 33 (2010) 465–473.
[74] K. Singh, M. Rani, V.K. Malik, N. Panwar, Structural, Optical, Magnetic, and Magnetocaloric Properties of $Sn_2Mn2O_7$ Pyrochlore, Phys. Status Solidi Appl. Mater. Sci. 221 (2024) 1–9.
[75] M.K. Sharma, A. Kumar, K. Kumari, S.J. Park, N. Yadav, S.H. Huh, B.H. Koo, Evidence of Hysteresis Free Ferromagnetic Nature and Significant Magnetocaloric Parameters in FeNi Binary Alloy, Magnetochemistry. 9 (2023) 1–14.
[76] Y. Zhang, B. Zhang, S. Li, J. Zhu, B. Wu, J. Wang, Z. Ren, Cryogenic magnetic properties and magnetocaloric effects (MCE) in B-site disordered $RE_2CuMnO_6$ (RE = Gd, Dy, Ho and Er) double perovskites (DP) compounds, Ceram. Int. 47 (2021) 18205–18212.